

GEOLOGIC MAP OF THE HARTS LAKE 7.5-MINUTE QUADRANGLE, PIERCE AND THURSTON COUNTIES, WASHINGTON

by Trevor A. Contreras, Rebecca L. Goughnour, and Todd R. Lau

WASHINGTON
GEOLOGICAL SURVEY
Map Series 2023-04
December 2023

INTERNALLY REVIEWED



WASHINGTON STATE DEPARTMENT OF
NATURAL RESOURCES
WASHINGTON GEOLOGICAL SURVEY

GEOLOGIC MAP OF THE HARTS LAKE 7.5-MINUTE QUADRANGLE, PIERCE AND THURSTON COUNTIES, WASHINGTON

by Trevor A. Contreras, Rebecca L. Goughnour, and Todd R. Lau

WASHINGTON
GEOLOGICAL SURVEY
Map Series 2023-04
December 2023

*This geologic map was funded in part by
the USGS National Cooperative Geologic
Mapping Program, award no. G22AC00364*

*This publication has been subject to an iterative technical review
process by at least one Survey geologist who is not an author.
This publication has also been subject to an iterative
review process with Survey editors and cartographers.*



WASHINGTON STATE DEPARTMENT OF
NATURAL RESOURCES
WASHINGTON GEOLOGICAL SURVEY

DISCLAIMER

Neither the State of Washington, nor any agency thereof, nor any of their employees, makes any warranty, express or implied, or assumes any legal liability or responsibility for the accuracy, completeness, or usefulness of any information, apparatus, product, or process disclosed, or represents that its use would not infringe privately owned rights. Reference herein to any specific commercial product, process, or service by trade name, trademark, manufacturer, or otherwise, does not necessarily constitute or imply its endorsement, recommendation, or favoring by the State of Washington or any agency thereof. The views and opinions of authors expressed herein do not necessarily state or reflect those of the State of Washington or any agency thereof.

INDEMNIFICATION

Research supported by the U.S. Geological Survey, National Cooperative Geologic Mapping Program, under USGS award number G22AC00364. The views and conclusions contained in this document are those of the authors and should not be interpreted as necessarily representing the official policies, either expressed or implied, of the U.S. Government.

WASHINGTON STATE DEPARTMENT OF NATURAL RESOURCES

Hilary S. Franz—*Commissioner of Public Lands*

WASHINGTON GEOLOGICAL SURVEY

Casey R. Hanell—*State Geologist*

Jessica L. Czajkowski—*Assistant State Geologist*

Ana Shafer—*Assistant State Geologist*

Washington State Department of Natural Resources Washington Geological Survey

Mailing Address:

1111 Washington St. SE

MS 47007

Olympia, WA 98504-7007

Street Address:

Natural Resources Bldg, Rm 148

1111 Washington St SE

Olympia, WA 98504

Phone: 360-902-1450

Fax: 360-902-1785

Email: geology@dnr.wa.gov

Website: <http://www.dnr.wa.gov/geology>

Publications and Maps:

[www.dnr.wa.gov/programs-and-services/geology/](http://www.dnr.wa.gov/programs-and-services/geology/publications-and-data/publications-and-maps)

[publications-and-data/publications-and-maps](http://www.dnr.wa.gov/programs-and-services/geology/publications-and-data/publications-and-maps)



Washington Geology Library Searchable Catalog:

[www.dnr.wa.gov/programs-and-services/geology/](http://www.dnr.wa.gov/programs-and-services/geology/washington-geology-library)

[washington-geology-library](http://www.dnr.wa.gov/programs-and-services/geology/washington-geology-library)

Suggested Citation: Contreras, T. A.; Goughnour, R. L.; Lau, T. R., 2023, Geologic map of the Harts Lake 7.5-minute quadrangle, Pierce and Thurston Counties, Washington: Washington Geological Survey Map Series 2023-04, 1 sheet, scale 1:24,000, with 16 p. text. [https://www.dnr.wa.gov/publications/ger_ms2023-04_geol_map_harts_lake_24k.zip]

Cover image: Large 4-m-tall andesite boulder found in landscaping 400 m north of Harts Lake. Boulder may have been transported in volcanic mudflows prior to the advance of the most recent continental ice sheet. Photo by T. Contreras.



TREVOR A. CONTRERAS

Trevor A. Contreras
December 2023

Contents

Introduction	1
Geologic Overview	1
Unlithified Pleistocene Deposits	1
Regional Structure and Volcanic Hazards	2
Methods	3
Geologic Mapping	3
Geochronology	3
Potential-Fields Geophysical Methods	3
Description of Map Units	4
Holocene to Pleistocene Post-Glacial Deposits	4
Late Pleistocene Glacial and Interglacial Deposits	4
Tertiary Bedrock Units	6
Discussion	7
Differentiating Between Qpc and Mashel Formation Based on Age	7
Arsenic in Wells That Encounter Qpc	7
Geophysics and Structures	7
Acknowledgments	9
Worker Contributions	9
References	9
Appendix A. Geophysical Methods	12
Appendix B. Luminescence Age Estimates	15

FIGURES

Figure 1. Regional map of the southern Puget Lowland	2
Figure 2. Arsenic concentrations at private water wells within the Harts Lake quadrangle....	8

TABLES

Table 1. Summary of geochronology	5
Table B1. Optically Stimulated Luminescence (OSL) and Infrared Stimulated Luminescence (IRSL) results from age sites GD1 and GD5	15

MAP SHEET

Geologic map of the Harts Lake 7.5-minute quadrangle,
Pierce and Thurston counties, Washington

Figure M1. Geophysical interpretation for the map area

Geologic Map of the Harts Lake 7.5-minute Quadrangle, Pierce and Thurston Counties, Washington

by Trevor A. Contreras¹, Rebecca L. Goughnour¹, and Todd R. Lau¹

¹ Washington Geological Survey
1111 Washington St SE
MS 47007
Olympia, WA 98504-7007

ABSTRACT

We present a geologic map of the Harts Lake quadrangle in Washington's southern Puget Lowland. We combine new geologic mapping, well log data, and geophysical modeling to better understand the glacial history, volcanic hazards, and local faulting in the map area. Quaternary glacial drift covers most of the map area, with a veneer of ablation till covering most of the glaciated and fluted surfaces. We interpret deposits along the Nisqually River and Tanwax Creek that were previously mapped as Miocene Mashel Formation (Walters, 1965) as younger Pleistocene lahars and alluvium from the Cascade Range. A review of cuttings and well logs from the E.F.E. Willhoite et al. No.1 oil exploration well, drilled by the Humble Oil & Refining Company in 1961, helped inform the cross section and geophysical model for the quadrangle, providing new insight into the structure of the subsurface. Some water wells in the southeast portion of the map area produce water with arsenic concentrations above the Washington State Department of Health's recommendations for drinking water. We believe that the high concentration of arsenic in these wells may be related to the decay of organic material that was preserved by Pleistocene or older Pliocene–Miocene volcanic mudflow deposits.

INTRODUCTION

The map area is located approximately 35 km east of Olympia near McKenna in the southern Puget Lowland (Fig. 1). The landscape of the Harts Lake quadrangle was sculpted by the Cordilleran ice sheet during the most recent glacial advance ~16,000 years ago. The southern limit of the ice sheet reached to approximately the Deschutes River south of the map area (Fig. 1). The map area is northeast of the Olympia structure—a gravity and magnetic lineament first noted by Daneš and others (1965) and recently interpreted as a fault by Polenz and others (2021, 2022). Mount Rainier lies approximately 30 mi east of the map area (Fig. 1).

The Nisqually River passes through the southwestern corner of the map area and State Route 702 crosses the central portion of the map area; State Route 7 lies just east of the quadrangle. Within the map area, land is primarily used for rural residences, forestry, and agriculture. Historically, borrow pits have produced construction aggregate from glacial outwash for local use.

This publication provides insight into geologic hazards (earthquakes, landslides, and lahars) and natural resources (water and aggregate). It provides information about rock types, properties, ages, and the processes that formed the landscape—from Pleistocene Mount Rainier lahar deposits in the southern portion of the map area, to Pleistocene glacial scour and deposition by

the continental ice sheet, and post-glacial incision and alluvial deposition by the Nisqually River. New geophysical data and modeling provide evidence of Eocene extension and possibly related volcanism in basement material beneath the Quaternary cover, as previously suggested by Wells and others (2014). This map builds on prior mapping in and near the study area that began in the 20th century (Bretz, 1913; Mundorff and others, 1955; Wallace and Molenaar, 1961; Noble and Wallace, 1966; Walters and Kimmel, 1968; Schasse, 1987; Polenz and others, 2021, 2022).

GEOLOGIC OVERVIEW

Unlithified Pleistocene Deposits

Glacial deposits cover most of the map area with sediment derived from the Cascade Range, the San Juan Islands, and the Coast Mountains of British Columbia (Armstrong and others, 1965). Most of this lithologically diverse drift was transported into the map area by Cordilleran glacial ice and meltwater during the late Wisconsinan Vashon stade of the Fraser Glaciation, when ice reached its southern terminus just south of the map area (Bretz, 1913; Noble and Wallace, 1966; Polenz and others, 2022; Fig. 1).

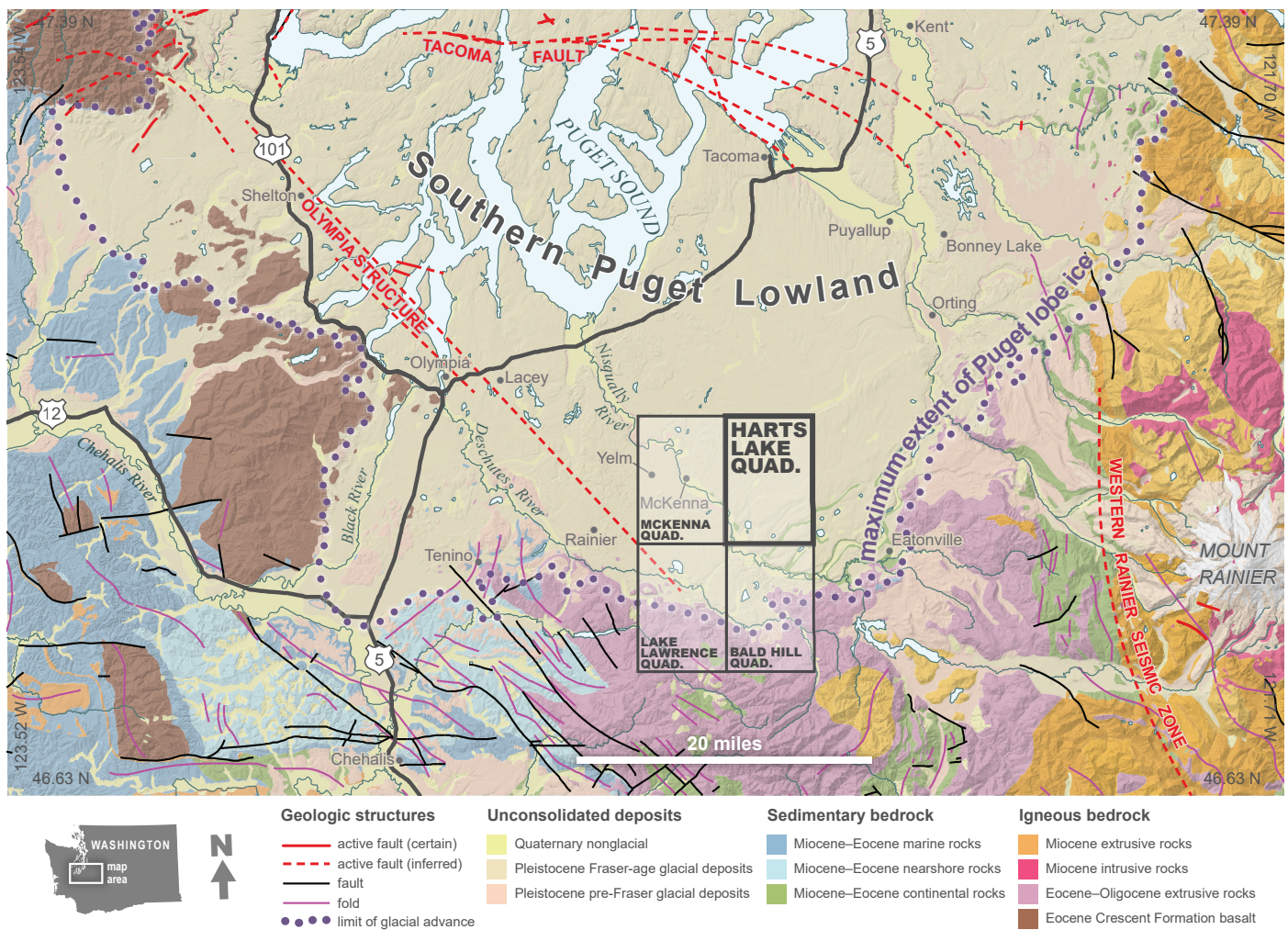


Figure 1. Regional map of the southern Puget Lowland showing surface geology, tectonic structures, and place names in the vicinity of the Harts Lake quadrangle. QUAD. is short for quadrangle.

Radiocarbon dates suggest that the ice advanced gradually, collapsed quickly, and was only present in the area between about 15.3 and 16 ka (Polenz and others, 2015; Haugerud, 2021).

The ancestral and modern Nisqually River and lahars moved sediment westward from the Cascade Range into the map area, with sediment pulses likely responding to both volcanic activity and Pleistocene glaciations of Mount Rainier and surrounding areas (Walters and Kimmel, 1968; Crandell and Miller, 1974; Sisson and others, 2001; Walsh and others, 2003; Polenz and others, 2022, 2023).

Glacial scour and deposition from continental ice and meltwater led to a patchwork of geomorphic features identifiable in lidar imagery. In the map area, drumlins and flutes record southwestward ice movement, while kettles and eskers mark where stagnant ice wasted away (as in Haugerud, 2009; and Polenz and others, 2009), and outwash channels and terraces document meltwater pathways (as in fig. 3 of Logan and others, 2009) and post-glacial Nisqually River incision.

Regional Structure and Volcanic Hazards

A northwest-trending, northeast-down gravity gradient and a set of broadly northwest-trending aeromagnetic lineaments extend from the Olympic Mountains to the Bald Hill quadrangle south

of the map area (Fig. 1). This gravity anomaly was first noted by Daneš and others (1965) and has been called the Olympia structure by later workers (Odum and others, 2016). Recent geologic mapping and modeling of the magnetic and gravitational fields in the McKenna and Lake Lawrence quadrangles (Fig. 1) suggest that the Olympia structure is a fault with primarily normal displacement (Polenz and others, 2022).

The Olympia fault is the southwestern edge of the Tacoma basin. Northeast of the Olympia fault, the Tacoma basin has an estimated depth of 5–7 km (Pratt and others, 1997; Brocher and others, 2001; Van Wagoner and others, 2002) and is bounded by the active Tacoma fault in the north (Brocher and others, 2001; Nelson and others, 2008). While faults spatially associated with the Olympia structure have shown postglacial movement northwest of Olympia (Clement and others, 2010; Odum and others, 2016), no Quaternary tectonic deformation has been clearly attributed to the Olympia fault on the southeast end, near the map area.

Lahar deposits and volcanic sediment-rich alluvium derived from Mount Rainier and the ancestral Cascade Range have been deposited throughout the Pleistocene to the present and are exposed in the map area, particularly in the south along the Nisqually River. Pumice fragments in the alluvium along the Nisqually River show evidence of deposition by lahars over

the last few thousand years. Polenz and others (2023) identified ~2,500-year-old lahar deposits just over 1 km south of the map area in the Bald Hill quadrangle, and Polenz and others (2022) mapped lahar and lahar runout deposits near McKenna (Fig. 1).

METHODS

Geologic Mapping

We identified units from field observations in the Harts Lake quadrangle in the summer and fall of 2022. We collected field data and constructed preliminary field-based maps using tablets equipped with GPS. We refined our field mapping through petrographic review of thin sections, radiocarbon dating, luminescence dating, geophysical measurements, analysis of well and boring records, and consideration of prior geologic mapping, aerial orthophotos, and geomorphic features identified from lidar. We used a lidar-based digital elevation model (DEM) with a 2-m grid resolution (Puget Sound Regional Council, 2005; U.S. Geological Survey, 2016; Pierce County, WA, 2020; Washington Department of Natural Resources, 2021) to estimate site elevations and derive hillshade images and other products.

To assist in mapping peat deposits that were historically drained for agricultural production, we used compiled soil survey mapping (Department of Natural Resources, unpublished soils geospatial data, 2023). Edge mismatches with the adjacent McKenna quadrangle (Polenz and others, 2022) are intentional based on insights from our latest mapping. We report measurements and data using the metric system; the one exception is elevation, which we report in feet-above-sea-level (ft).

During our mapping, we collected ~600 new outcrop observations and made 42 thin sections to differentiate provenance, verify lahar deposits, and to better identify and describe the geologic units. To better constrain subsurface conditions for the mapping and cross section, we reviewed ~1,000 well and boring records from the Department of Ecology's well log database (Washington State Department of Ecology, 2022), relocating 255 of them based on parcel number and (or) well address.

We infer much of the cross section from geophysical modeling (Fig. M1A and M1B), water-well logs, and an oil exploration well (E.F.E. Willhoite et al. No. 1, API Number: 046-053-00006; hereafter referred to as the Willhoite well) that the Humble Oil & Refining Company drilled in the central portion of the map area to a depth of 1,744 meters in 1961. We accessed original files and reports for the Willhoite well (Washington Geological Survey, Oil and Gas files-WA File Number 157, 2023) from the Washington Geological Survey (WGS) Oil and Gas database (Washington Geological Survey, 2019). We also retrieved the washed cuttings for the Willhoite well from our core facility to review lithologies encountered in the well.

We acquired countywide water quality data from the Tacoma–Pierce County Health Department. These data include the locations of wells (Fig. 2) tied to specific parcels, and arsenic concentrations as reported from test results (Tacoma–Pierce County Health Dept., written commun., 2023).

Geochronology

We used luminescence dating (see Appendix B) to constrain the depositional age of pre-Vashon sediment exposed directly under Vashon-age stagnant-ice deposits. We collected luminescence samples utilizing online instructions from Utah State University's Luminescence Lab on how to sample (Utah State University Luminescence Lab, 2022). Three samples collected during the field season were analyzed by the U.S. Geological Survey (USGS) Luminescence Dating Laboratory in Denver, Colorado.

We used one luminescence date that was reported by Polenz and others (2022) in their publication for the McKenna and Lake Lawrence quadrangles (Fig. 1). Note that the date was not shown on their map because the sample is located within the Harts Lake quadrangle. Likewise, our OSL date GD6 is not shown on our map plate because it is in the adjacent McKenna quadrangle.

We used radiocarbon dating to differentiate pre-Vashon sediments from Holocene deposits. Organic samples were collected, dried, and manually cleaned to remove potential contamination. They were weighed, packaged, and shipped to two commercial carbon dating companies utilizing their sample submission recommendations (DirectAMS, 2023). Both Beta Analytic and DirectAMS laboratories were utilized.

Potential-Fields Geophysical Methods

We collected 347 new gravity observations using a Scintrex model CG-6 gravimeter and combined these with 953 points from previous studies (WGS unpublished data, 2021; PACES dataset; Polenz and others, 2021, 2022) to make a new isostatic anomaly map (contours on Fig. M1A). Our methods for collecting gravity data are outlined in Appendix A and the gravity data are listed in the Data Supplement. We collected gravity measurements outside of the map area to prevent introducing gridding edge effects into our interpretations (Fig. M1A). In addition, we applied a quantitative algorithm to select high-amplitude, linear gradients in the gravity data for interpretation (called 'max-spots'; Appendix A; Fig. M1A). We also used aeromagnetic data from two surveys (Blakely and others, 1999, 2020) to interpret magnetic anomalies related to volcanic bedrock and lineaments possibly related to faults or folds.

We employed forward modeling of the gravity and aeromagnetic data along Cross Section A–A' using GM-SYS (Seequent, Inc.) to produce a quantitatively tested interpretation of the subsurface on which we could base our geologic cross section. We produced a geophysical model (Fig. M1B) through an iterative process of adjusting model geometries to fit potential field observations and surficial geological constraints, which in turn informs the geologic cross section. We calibrated our modeling parameters for local geologic units with published and unpublished rock properties (WGS unpublished; Polenz and others, 2022), and with 49 new density and 316 new magnetic susceptibility measurements. These new measurements are included in the data supplement associated with this map.

DESCRIPTION OF MAP UNITS

Holocene to Pleistocene Post-Glacial Deposits

- ml Modified land (Holocene)**—Varied amounts of locally derived soil, gravel, sand, silt, and clay; excavated and (or) redistributed to modify topography for agricultural and industrial developments, including but not limited to gravel pits, ponds, and canal infrastructure. Excludes small or shallow reworking (less than 1.5 m deep or thick), such as most residential sites and road-related modifications. Primarily mapped based on topographic expression in lidar data.
- Qp Peat (Holocene to Pleistocene)**—Organic and organic-rich sediment, includes peat, gyttja, muck, silt, clay, and sand; typically deposited in kettles, areas between drumlins, abandoned drainages, or other poorly drained flat areas; mapped where lidar reveals such landforms and in areas where we interpret hydrophilic vegetation or wet conditions without trees based on aerial photos. Land use in the region has resulted in the drainage of some previously wet areas; for these areas, we rely on aerial photos, lidar data, and soil surveys to identify soils that may have been perpetually water-logged. The soil surveys often describe these soils as having a parent material of “mucks,” and the lidar data show these areas as flat and low-lying with linear drainage ditches.
- Qa Alluvium (Holocene to Pleistocene)**—Unconsolidated gravel, sand, silt, and peat in varied amounts; mapped in active river and stream channels and floodplains. Deposits of unit Qa along the Nisqually River are primarily reworked andesitic material shed from Mount Rainier, with rare pumice fragments similar to those found upstream in Holocene lahar deposits (Polenz and others, 2023). Along Tanwax Creek, alluvium deposits are patchy and scoured down to the underlying unit Qpc in some places. Alluvium is mapped from lidar data.
- Qaf Alluvial fan (Holocene to Pleistocene)**—Varied amounts of pebble- to cobble-gravel and sand with minor silt; generally unconsolidated and poorly sorted; thickness was not determined while mapping; mapped where stream channels open up into unconfined topography and a characteristic fan-shaped morphology can be observed in lidar. Some mapped fans may not be active in the current climatic regime; however, we were unable to differentiate these from currently active fans due to a lack of obvious incision or activity in lidar and orthophotos. Further differentiation may require site-specific studies. Unit Qaf is post-glacial in age.
- Qls Landslide deposits (Holocene to Pleistocene)**—Sand, silt, clay, pebbles, cobbles, and boulders, in varied amounts, derived from deposits upslope; mostly loose, unsorted, and jumbled; mapped from landforms expressed in lidar. Abundant landslides along Tanwax

Creek suggest that the underlying material, unit Qpc, is particularly landslide-prone on the south side of the creek. We infer that unit Qls is post-glacial in age because glaciation would have destroyed many older Qls deposits within the map area. Absence of a mapped landslide does not indicate the absence of landslide hazard.

- Qmw Mass-wasting deposits (Holocene to Pleistocene)**—Loose soil, gravel, sand, silt, and clay, all in varied amounts, deposited by shallow ravel and soil creep; locally includes colluvium, small landslides, and alluvial fans; thickness is poorly constrained but is likely ~1–5 m based on estimates from lidar data; deposits lie along the base of steep slopes throughout the quadrangle; identified from lidar and shown where colluvium covers the underlying units. Unit Qmw is post-glacial in age.

Late Pleistocene Glacial and Interglacial Deposits

The Puget Lobe of the Cordilleran ice sheet advanced from Canada to its southern terminus just south of the map area (Bretz, 1913; Polenz and others, 2023) during the late Wisconsinan Vashon stage of the Fraser Glaciation (Armstrong and others, 1965). We estimate that Vashon ice and all associated Vashon Drift entered the map area between about 15.3 and 16 ka, based on Polenz and others (2015—see their fig. 3 and discussion). The Vashon-age Puget ice lobe was divided into western (Olympia) and eastern (Yelm) lobes (Bretz, 1913; Noble and Wallace, 1966; Walsh and others, 2003; Polenz and others, 2021). Vashon Drift in the map area is from the Yelm Lobe.

VASHON DRIFT

- Qgo Recessional outwash, undivided (late Pleistocene)**—Pebble-gravel, less commonly cobble- and boulder-gravel, pebbly sand, or sand; light tan-brown to light gray-brown, or variegated with iron and silica cement; loose; well-rounded to subrounded; moderately sorted to well-sorted; gravel is clast-supported but locally with a matrix of sand and silt and interbeds of silt and sand; otherwise massive. Observations of exposures in borrow pits suggest a thickness of 3–10 m is common. Mapped in gently sloping outwash channels and stratigraphically above other Vashon glacial deposits (unit Qgic) and older units (unit Qpc) that the outwash and subglacial meltwater cut into. We query unit Qgo where outwash deposits exist but do not appear to be within obvious outwash channels as seen in lidar. Sometimes used for aggregate. Locally, the unit is subdivided into:
- Qgog Recessional outwash gravel (late Pleistocene)**—Cobble- to pebble-gravel with minor sand and (or) silt; tan to light brown; loose; ; subrounded; moderately sorted; found in outwash channels in the northern and central portions of the map area; a patchy silica coating on some clasts marks where the clasts were in contact. Unit Qgog is sometimes used for

Table 1. Summary of geochronology and co-located samples. Uncertainties are provided at 2-sigma (95%) confidence.

Sample	Interpreted Geologic Unit	Dating Method	Age	Age Type	Material	Co-located analyses
GD1	Qps	Luminescence	80.18 ±7.5 ka	Burial	Sand	none
GD2	NA*	¹⁴ C	modern	Maximum depositional age	Leaf	none
GD3	Qa	¹⁴ C	20 ±30 cal yr BP	Maximum depositional age	Wood	none
GD4	Qpvl	Luminescence	142.6 ±38.2 ka†	Burial	Sand	none
GD5	Qpvl	Luminescence	30.38 ±5.18 ka	Burial	Sand	TS28
GD6‡	Qpc	Luminescence	24.12 ±4.65 ka	Burial	Sand	none

* Not applicable, Float collected from disturbed modern soil.

† Luminescence date from Polenz and others (2022; their GD2).

‡ Not shown on map plate because sample is located outside and west of the map boundary.

aggregate. Some outwash in Rocky Slough and Tanwax Creek includes andesitic boulder deposits from a late-glacial flood known as the Tanwax flood, which occurred when an ice dam broke and led to the sudden drainage of a glacial lake northeast of the map area (Pringle and Goldstein, 2002; Polenz and others, 2021).

Qgos **Recessional outwash sand (late Pleistocene)**—Sand with minor silt and rare pebble-gravel; sand is mostly fine- to medium-grained quartz and lithics; tan to brown; generally loose; angular to subangular; moderately to well-sorted; found in the northwest corner of the map area; deposited on top of unit Qgic; unit Qgos is observed in areas with flat or subdued topography and in low-lying areas between fluted deposits of unit Qgic.

Qge **Eskers (late Pleistocene)**—Sandy pebble- to cobble-gravel and diamict; tan to light brown; clasts are subangular to rounded; moderately sorted; mapped where narrow, sinuous ridges are visible in lidar imagery; usually found adjacent to, or on top of, deposits of unit Qgic. Deposited by meltwater in subglacial or englacial channels as the ice sheet stagnated and melted (Benn and Evans, 1998). Sometimes used for aggregate.

Qgic **Ice contact deposits (late Pleistocene)**—Undivided stagnant ice deposits, consisting of ablation till, kame deposits, subglacial outwash, and rare lodgment till; primarily loose to compact silty diamict, with minor sandy pebble- to cobble-gravels; color is generally light gray to light brown-gray; grain-size in the diamict ranges from silt to boulder; clasts are generally sub-rounded; typically a chaotic mixture of variably sorted and bedded sediment and diamict; forms a veneer up to 10–15 m thick; clast lithology is diverse and includes rare metamorphics and granitoids, which suggest a northern provenance. The topographic character of unit Qgic includes drumlins and irregular hummocky landforms, such as kames and kettles that suggest the unit was deposited as the ice sheet stagnated and melted. Unit Qgic blankets older deposits of pre-Vashon

alluvium and lahar deposits (units Qpc and Qps). In the southeastern corner of the map area, unit Qgic appears to incorporate clay and andesite clasts derived from the underlying unit Qpc, which is not observed in the northern portion of the map area. We infer the age of unit Qgic to be about 16 ka, based on Polenz and others (2015).

Qgt? **Lodgment till (late Pleistocene)**—Diamict containing boulders, cobbles, sand, and an unsorted or poorly sorted matrix composed of sand- to clay-sized particles, all in varied amounts; clast lithology is diverse and contains rare, northern-sourced metamorphic and granitoid clasts; thickness is unknown, but likely less than a meter or two based on observations of till-like diamict we observed within the quadrangle. Unit Qgt? is deposited directly by glacial ice and usually includes a loose, surficial cover of 0.5–3 m of ablation till. We chose to query these polygons because we did not find exposures thick enough to be geotechnically significant or common in the map area. The few exposures where we observed lodgment till it was less than 0.5 m thick and would not appear to prohibit excavations. In surrounding quadrangles, Polenz and others mapped extensive lodgment till based on exposures and observations of smooth, well-developed drumlins in lidar. However, we did not observe lodgment till extensively enough to map, though we do extend a few designations of unit Qgt? into the map area along the western and southern border based on observations made by Polenz and others (2022, 2023) and information received during mapping (Michael Polenz, oral commun., 2023). Unit Qgt? is deposited on top of unit Qpc and has an age of about 16 ka, as inferred by Polenz and others (2015).

UNDIFFERENTIATED GLACIAL AND INTERGLACIAL SEDIMENTS

Qguc **Pre-Vashon glacial and nonglacial undifferentiated sediment (Pleistocene) (cross section only)**—Undivided sediment consisting of diamict, till, clay, silt, sand, pebble- to cobble-gravel, and occasional wood; interbedded with thick layers of orange, brown, and blue

clay and silty/sandy clay; classified as hard or dense according to the Unified Soil Classification System. We interpret unit **Qguc** as a combination of glacial and nonglacial sediment, including dense, clayey, pre-Vashon alluvium and lahars (unit **Qpc**). Unit **Qguc** is Pleistocene; however, due to the similarities between units **Qpc** and **RMc** and limited information from well logs, the contact between units **Qguc** and **RMc** is uncertain. **Qguc** is inferred from well logs and shown in cross section only.

Qps **Pre-Vashon sandy deposits (Pleistocene)**—Sand with rare pebbles; tan to gray; loose; moderately sorted fine to medium sand with minor silt; angular to subangular sand and subrounded pebbles; beds appear massive in isolated exposures; sand is quartz-rich and pebbles are of diverse lithologies, including rare metamorphic clasts which we interpret as having been transported from the North Cascades or British Columbia by a Cordilleran ice advance; approximately 7–10 m thick based on well logs and limited exposures; found in the northeaster portion of the map area; unit **Qps** is observed directly under diamicton of unit **Qgic** and is interpreted to be Pre-Vashon-age nonglacial fluvial sediment or proglacial outwash deposited by an advancing Puget Lobe ice sheet in a glaciofluvial or lacustrine setting. A luminescence age from this unit yielded an age of 80.18 ± 7.5 ka (Table 1, GD1). This date suggests the sediment correlates to the Whidbey Formation (marine isotope stage 5) of Easterbrook and others (1967) or early outwash of the Possession Drift (marine isotope stage 4) as described in Troost (2016).

PRE-VASHON SEDIMENT

Qpc **Pre-Vashon alluvium and lahar deposits from the Cascade Range, undivided (late Pleistocene)**—Boulder- to pebble-gravel and -diamicton, sand, silt, and clay; most clasts are andesite from the Cascade Range; variably colored, including pale-gray, light-brown, yellow-brown, and blue-gray; slightly weathered; compact and very stiff; sand usually rich in plagioclase, andesite lithics, and glassy volcanic fragments that alter to clay; unsorted to well sorted; typically well bedded; at least 60 m thick; mapped in the southern half of the map area and best exposed along the Nisqually River and Tanwax Creek. Based on an abundance of volcanic clasts and poor sorting, we interpret nearly all diamicton deposits within unit **Qpc** to be lahar or lahar runout deposits from Mount Rainer. The upper portion of the unit contains large andesite boulders (>3 m diameter), Polenz and others (2022) interpret these andesite boulders as being deposited by volcanic mudflows.

Unit **Qpc** is under Vashon glacial drift and may have been partially eroded by the Vashon ice sheet. Based on exposures along the Nisqually River to the southeast of the map area, unit **Qpc** appears to lie on older Pliocene to Miocene volcanoclastic deposits (Walters, 1965;

Polenz and others, 2023). Unit **Qpc** may contribute to high arsenic concentrations in groundwater, see Discussion. Within the map area, unit **Qpc** is estimated to be between 16 ka and 187.0 ± 58.6 ka (GD4). The 16 ka is a minimum age based on the overlying glacial drift, and we suspect unit **Qpc** is entirely pre-Vashon based on dates down the Nisqually River (Walsh and others, 2003; Polenz and others, 2022). Two new dates (GD5 and GD6) taken from the upper portion of the unit, but beneath the bouldery interval that we interpret as a mudflow deposit, provide an age range of 16.5 ka to 35.6 ka. This would suggest that large catastrophic mudflows were emplaced prior to the advance of the Puget Lobe into the area. Unit **Qpc** is queried where we expected the unit to be at or close to the surface, but exposures were obscured by a veneer of Vashon glacial drift.

Tertiary Bedrock Units

RMc **Continental sediment (Pliocene to Miocene?) (cross section only)**—Interbedded clay, silt, sand, medium-coarse gravel, and peat; sand and gravel contain primarily Cascade-sourced volcanic clasts and grains, including ash, pumice, and andesite. Stratigraphy in unit **RMc** closely resembles the type section of the Mashel Formation (Walters, 1965), which is located ~4 km southeast of the map area. Based on nearby exposures of unit **RMc** south of the map area (Polenz and others, 2023) and geophysical modeling, we infer unit **RMc** beneath the Harts Lake quadrangle. We infer a broad age range for this unit based on nearby work and that the Mashel Formation is defined as Miocene (Walters, 1965), but recent work established that similar deposits between the type section and our map area are as young as Pliocene (Polenz and others, 2023). Additional geochronologic analysis is needed to verify the age of this unit.

ØEn **Nearshore sedimentary rocks (Oligocene to late Eocene) (cross section only)**—Tuffaceous, silty, and sandy claystone with minor subangular volcanic and siliceous pebbles; described as “greenish-gray” in the Willhoite well log and appears light tan to buff in well cuttings; approximately 160 m thick based on descriptions in the Willhoite well log. Based on regional geologic context and geophysical modeling (Fig. M1B), we interpret unit **ØEn** to be part of the deltaic depositional system associated with the Puget Group (Snively and others, 1958).

Ev_n **Volcanic and volcanoclastic rocks, undivided (late to middle Eocene) (cross section only)**—Reported as interbedded basalt and volcanoclastic sedimentary rock in the Willhoite well log. Basalt is brown, black, red, gray, purplish, and greenish in color, and is porphyritic to aphanitic, locally with vesicles. Volcanoclastic sedimentary rock consists of lithic tuff and crystal-rich claystone, siltstone, and minor sandstone. Unit **Ev_n** has

an apparent thickness of ~1,400 m based on lithologic descriptions in the Willhoite well log. We measured magnetic susceptibility of well cuttings from the Willhoite well; these measurements are consistent with susceptibility measurements from Northcraft Formation andesite collected by Polenz and others (2021, 2022, 2023). Based on these measurements and previous geophysical modeling of Northcraft Formation andesite at depth in the region (Polenz and others, 2022), we interpret the volcanic rocks in the Willhoite well to be part of the Northcraft Formation (Snively and others, 1951).

DISCUSSION

In this section we discuss the challenge of differentiating unit Qpc from the Mashel Formation, identify a possible geologic explanation for elevated arsenic concentrations in groundwater, and present the results of our geophysical modeling.

Differentiating Between Qpc and Mashel Formation Based on Age

Previous workers have mapped Miocene Mashel Formation along Tanwax Creek and tentatively along the Nisqually River (Walters and Kimmel, 1968; Schasse, 1987). We chose to map these deposits as Pleistocene pre-Vashon alluvium and lahars from the Cascade Range (unit Qpc) based on dating by Polenz and others (2022). It can be difficult to distinguish between deposits of Mashel Formation and unit Qpc because both units consist of interbedded lahar deposits, sand, clay, and gravel with a primarily volcanic source of sediment. Polenz and others (2022) collected a luminescence date at the base of a 55 m section along the Nisqually River within the Harts Lake quadrangle that suggests deposition occurred at 187.0 ± 58.6 ka at this site (their age site GD2; reported in this publication as GD4). Additionally, a detrital zircon age sampled at the same location (GD3 in Polenz and others, 2022) requires deposition after ~1 Ma. These Pleistocene ages suggest that deposits of unit Qpc may be considerably younger than the Miocene Mashel Formation, and instead consist largely of alpine glacial outwash deposited during growth stages of Mount Rainier (Sisson and others, 2001).

Arsenic in Wells That Encounter Qpc

As shown in Figure 2, approximately 60 out of 1,000 water wells in the map area produce water with arsenic concentrations that exceed Washington State Department of Health recommendations of less than 10 ppb (parts per billion; Washington State Dept. of Health, 2014). Nearly all of them are in the southern half of the map area and utilize aquifers within or below the Pleistocene alluvium and lahars from the Cascade Range (unit Qpc). Arsenic concentration and well-location data from Tacoma–Pierce County Health Department are depicted in Figure 2, which shows arsenic concentrations for wells in the map area, and highlights wells that exhibit concentrations above the 10 ppb limit (Tacoma–Pierce County Health Dept., written commun., 2023). Based on the test results and comparison with well logs

(Washington State Dept. of Ecology, 2022), we found these wells were often drilled through 30 to 100 m of clay-rich deposits that we interpret as altered volcanic sediment. Some well reports mention encountering wood while drilling, which suggests that they may be tapping into the underlying Mashel Formation, as mapped nearby by Polenz and others (2023), or Pleistocene lahars rich in preserved organic materials.

Two factors could be contributing to the elevated arsenic levels in this area; (1) reduced groundwater conditions from the oxidation of organic matter (San Juan, 2022), or (2) hydrothermally altered volcanic and sedimentary rocks that contain arsenic and which were transported from the Cascade Range following volcanic eruptions. Historically, arsenic and mercury were mined in two locations: along the Green River north of the map area, and at Cinebar south of the map area. At these mining locations, coal bearing sedimentary rocks of the Puget Group were intruded by andesite, depositing realgar, cinnabar, and calcite (Mackin, 1944; Hunting, 1956; Dillhoff and Dillhoff, 1991). Additional research could confirm how extensive these conditions (sedimentary rocks that have been intruded, and organic material covered up by lahars) are upstream, and the degree to which they could be contributing to the elevated arsenic levels.

Geophysics and Structures

New potential field data provide insight into the geologic material and structures beneath the extensive quaternary cover. Geophysical models (Finn, 1990; unpublished records, Washington Geological Survey (WGS)) indicate that in addition to the Northcraft Formation and interbedded Eocene and younger sediments, rocks in the subsurface of the map area include early Eocene Crescent Formation basalt of the Siletzia terrane (Wells and others, 2014; Eddy and others, 2016, 2017; Polenz and others, 2021, 2022).

POTENTIAL FIELD PATTERNS

The area with the lowest isostatic gravity is located in the northwest portion of the quadrangle, which we interpret to be the deepest part of the Tacoma Basin within our study area ('TBGL' in Fig. M1A). Isostatic gravity increases to the southeast corner of the quadrangle. Across the center portion of the quadrangle gravity contours trend north–northeastward, which we interpret as a sub-basin within the Tacoma basin. The gravity max spots form sinuous, discontinuous lines that trend southwest and delineate a northwest-down gravity gradient (EBF on Fig. M1A). We interpret the source of these anomalies as short, discontinuous northwest-down normal faults, which juxtapose basement Crescent Formation ($\rho = 2,880 \text{ kg/m}^3$) against less-dense basin sediment ($\rho = 2,295 \text{ kg/m}^3$).

A low-amplitude, long-wavelength anomaly dominates the rest of the quadrangle (green areas in Fig. M1A). We attribute this anomaly to thick (~6,500–9,000-ft-thick) sediment and pyroclastic material with relatively low magnetic susceptibility ($\chi = 25 \times 10^{-3} \text{ SI}$), which overlie the more-magnetic Crescent Formation basement ($\chi = 55 \times 10^{-3} \text{ SI}$).

MODELING RESULTS

Modeling for the Harts Lake quadrangle suggests two normal faults ('WBF' and 'EBF' on Fig. M1A) offsetting the Crescent

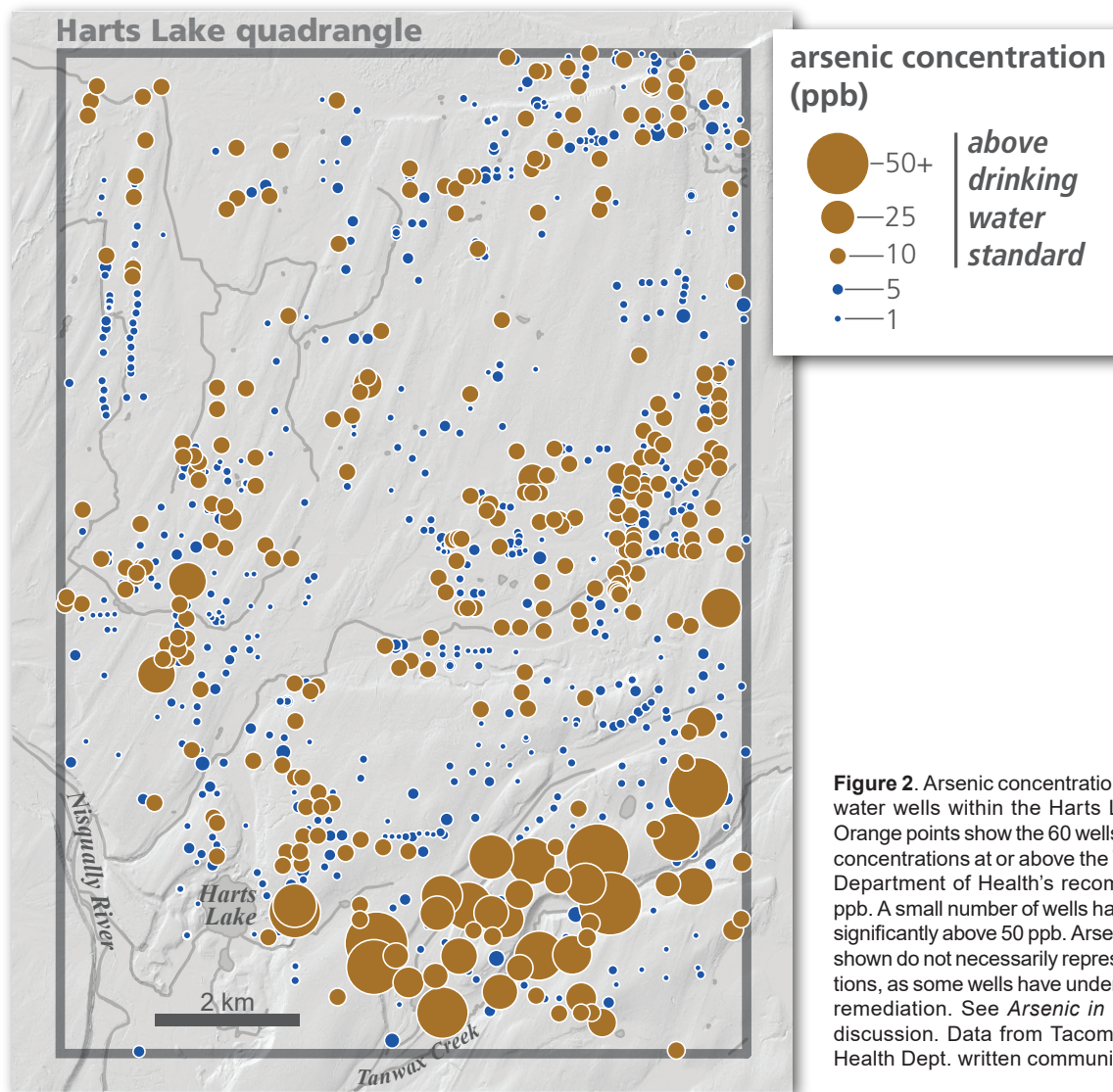


Figure 2. Arsenic concentrations at 1,100 private water wells within the Harts Lake quadrangle. Orange points show the 60 wells that have arsenic concentrations at or above the Washington State Department of Health’s recommendation of 10 ppb. A small number of wells have concentrations significantly above 50 ppb. Arsenic concentrations shown do not necessarily represent current conditions, as some wells have undergone subsequent remediation. See *Arsenic in Wells* section for discussion. Data from Tacoma–Pierce County Health Dept. written communication (2023).

Formation and Eocene Tacoma Basin sediments, which fits the isostatic anomaly well. Offset on these faults is down-to-the-north for the westernmost fault (WBF in Fig. M1A and M1B) and down-to-the-northwest for the southeasternmost fault. Normal offset with syntectonic thickening of Eocene basin sediments along moderately dipping (65–75 degrees) faults is well constrained by the modeling, and are a good fit to the observed potential field data.

Our modeling agrees with the previous modeling of Polenz and others (2021, 2022), which indicated that much of the basin is filled with low-density volcanic sediments interbedded with magnetic volcanic or volcanoclastic material (labeled as ‘volcanoclastic, andesite, and sedimentary interbedded mix’ on Fig. M1B). We constrain this material in our modeling from calculated magnetic susceptibility measurements from the Willhoite well using the mass susceptibility method outlined in Appendix A. The log from this oil well suggests that this material is mostly basalt and (or) basaltic andesite volcanoclastic material with interbedded tuff and sediment. We suspect these interbeds are more layered in the subsurface than our data and modeling can resolve. We represent this material as one geophysical block of interbedded volcanic material (unit Evs_N in Fig. M1A) with density

values taken from previous modeling ($\rho = 2,295 \text{ kg/m}^3$; Polenz and others, 2022) and magnetic susceptibility from calculated volume susceptibility of Willhoite well cuttings ($\chi = 20 \times 10^{-3} \text{ SI}$, Appendix A). We interpret that these volcanic bodies (‘Andesite flow or intrusion’ in Fig. M1B and ‘TBV’ in Fig M1A) originated from nearby volcanic sources (Polenz and others 2021, 2022, 2023) and (or) unidentified sources to the east of our study area.

BASIN STRUCTURE

A southwest-striking, curvilinear group of max spots (‘CLF’ in Fig. M1A) is likely produced by normal faulting of basin material related to northeastward extension along the Olympia fault (see Polenz and others, 2021, 2022, 2023). Continuity of the gravity max spots suggests that they relate to our modeled south to southwest-striking normal faults (‘WBF’ and ‘EBF’ in Fig. M1A). Within the Harts Lake quadrangle, a general pattern emerges from the potential fields that suggests northwest-down offset relative to the southeastern portion of the quadrangle. The gravity and magnetic lows (‘TBGL’ and ‘TBML’ in Fig. M1A) represent the deepest part of a local sub-basin of the greater Tacoma Basin, and the eastern blind fault (‘EBF’ in Fig. M1A) represents the eastern edge of the sub-basin.

ACKNOWLEDGMENTS

We thank: Pat Pringle, Tim Walsh (both WGS retired), Frank Hladky, and Michael Polenz for fielding questions about prior mapping; Michael Polenz for access to his data, reports, field assistance, and thoughtful reviews; Anita Bauer for field assistance, gravity data collection, assessment of rock density and magnetic susceptibility; Gabriel Legorreta Paulín of the Instituto de Geografía Universidad Nacional Autónoma de México Ciudad de México for providing supervised classification of Landsat data spectral analysis; Shannon Mahan of the USGS and Tabor Reedy at U.S. Bureau of Reclamation for luminescence dates; Alex Steely, Andrew Sadowski, Megan Anderson, and Logan Wetherell for helpful reviews; Katie Alexander for the GeMs database template; Daniel Coe, Nikolas Midttun, and Susan Schnur for drafting figures and editing along with all WGS staff who provided suggestions, edits, and guidance; the innkeepers at Two Frog Bog for lemonade on a very hot day; the city of Centralia, the Nisqually Land Trust, Joint Base Lewis–McChord, Wilcox Family Farms, Manke Timber Company, the Nippers, and countless other landowners for land access and local knowledge.

WORKER CONTRIBUTIONS

T. Lau performed geophysical data collection, modeling and writing pertaining to the geophysical work. R. Goughnour carried out geologic fieldwork and mapping in the northern half of the map area, constructed the cross section, examined thin sections, and drafted portions of the pamphlet text. T. Contreras functioned as project lead, drafted GIS features and the overall report, and led geologic fieldwork.

REFERENCES

- Ali, Arfan; Potter, D. K.; Tugwell, Andrew, 2015, Magnetic susceptibility of drill cuttings in a North Sea oil well: A rapid, nondestructive means of characterizing lithology: 2015 International Symposium of the Society of Core Analysts, St. John's, Newfoundland and Labrador, Canada, Paper SCA2015-036, 6 p. [<http://www.jgmaas.com/SCA/2015/SCA2015-036.pdf>]
- Armstrong, J. E.; Crandell, D. R.; Easterbrook, D. J.; Noble, J. B., 1965, Late Pleistocene stratigraphy and chronology in southwestern British Columbia and northwestern Washington: *Geological Society of America Bulletin*, v. 76, no. 3, p. 321–330. [[https://doi.org/10.1130/0016-7606\(1965\)76\[321:LPSACI\]2.0.CO;2](https://doi.org/10.1130/0016-7606(1965)76[321:LPSACI]2.0.CO;2)]
- Barnes, D. F.; Oliver, H. W.; Robbins, S. L., 1969, Standardization of gravimeter calibrations in the Geological Survey: *Eos Transactions*, v. 50, no. 10, p. 626–627. [<https://doi.org/10.1029/EO050i010p00526>]
- Benn, D. I.; Evans, D. J. A., 1998, *Glaciers and glaciation*: Edward Arnold (Hodder Headline Ltd.), Oxford University Press, 734 p.
- Blakely, R. J.; Wells, R. E.; Weaver, C. S., 1999, Puget Sound aeromagnetic maps and data: U.S. Geological Survey Open-File Report 99-514, version 1.0. [<http://geopubs.wr.usgs.gov/open-file/of99-514/>]
- Blakely, R. J.; Sherrod, B. L.; Weaver, C. S., 2020, High-resolution aeromagnetic survey of the Centralia area, southwest Washington: U.S. Geological Survey data release. [<https://doi.org/10.5066/P9T4UC6W>]
- Bretz, J. H., 1913, Glaciation of the Puget Sound region: *Washington Geological Survey Bulletin* 8, 244 p., 3 plates. [http://www.dnr.wa.gov/publications/ger_b8_glaciation_pugetsound.pdf]
- Brocher, T. M.; Parsons, T. E.; Blakely, R. J.; Christensen, N. I.; Fisher, M. A.; Wells, R. E.; SHIPS Working Group, 2001, Upper crustal structure in Puget Lowland, Washington: Results from the 1998 Seismic Hazards Investigations in Puget Sound: *Journal of Geophysical Research Solid Earth*, v. 106, no. B7, p. 13,541–13,564. [<https://doi.org/10.1029/2001JB000154>]
- Clement, C. R.; Pratt, T. L.; Holmes, M. L.; Sherrod, B. L., 2010, High-resolution seismic reflection imaging of growth folding and shallow faults beneath the southern Puget Lowland, Washington State: *Bulletin of the Seismological Society of America*, v. 100, no. 4, p. 1710–1723. [<https://doi.org/10.1785/0120080306>]
- Crandell, D. R.; Miller, R. D., 1974, Quaternary stratigraphy and extent of glaciation in the Mount Rainier region, Washington: U.S. Geological Survey Professional Paper 847, 59 p., 2 plates. [<https://doi.org/10.3133/pp847>]
- Daneš, Z. F.; Bonno, M. M.; Brau, E.; Gilham, W. D.; Hoffman, T. F.; Johansen, D.; Jones, M. H.; Malfait, B.; Masten, J.; Teague, G. O., 1965, Geophysical investigation of the southern Puget Sound area, Washington: *Journal of Geophysical Research*, v. 70, no. 22, p. 5573–5580. [<https://doi.org/10.1029/JZ070i022p05573>]
- Dillhoff, R. M.; Dillhoff, T. A., 1991, Realgar from the Royal Reward mine, King County, Washington: *Rocks and Minerals*, v. 66, no. 4, p. 310–314.
- DirectAMS, 2023, Radiocarbon dating wood, plant, & cellulose [webpage]: DirectAMS Radiocarbon Dating Service. [accessed June 12, 2023, at <https://www.directams.com/wood-plant-cellulose>]
- Easterbrook, D. J.; Crandell, D. R.; Leopold, E. B., 1967, Pre-Olympia Pleistocene stratigraphy and chronology in the central Puget Lowland, Washington: *Geological Society of America Bulletin*, v. 78, no. 1, p. 13–20. [[https://doi.org/10.1130/0016-7606\(1967\)78\[13:PPSACI\]2.0.CO;2](https://doi.org/10.1130/0016-7606(1967)78[13:PPSACI]2.0.CO;2)]
- Eddy, M. P.; Bowring, S. A.; Umhoefer, P. J.; Miller, R. B.; McLean, N. M.; Donaghy, E. E., 2016, High-resolution temporal and stratigraphic record of Siletzia's accretion and triple junction migration from nonmarine sedimentary basins in central and western Washington: *Geological Society of America Bulletin*, v. 128, no. 3–4, p. 425–441. [<https://doi.org/10.1130/B31335.1>]
- Eddy, M. P.; Clark, K. P.; Polenz, Michael, 2017, Age and volcanic stratigraphy of the Eocene Siletzia oceanic plateau in Washington and on Vancouver Island: *Lithosphere*, v. 9, no. 4, p. 652–664. [<https://doi.org/10.1130/L650.1>]
- Finn, C. A., 1990, Geophysical constraints on Washington convergent margin structure: *Journal of Geophysical Research Solid Earth*, v. 95, no. B12, p. 19,533–19,546. [<https://doi.org/10.1029/JB095iB12p19533>]
- Finn, C. A.; Phillips, W. M.; Williams, D. L., 1991, Gravity anomaly and terrain maps of Washington: U.S. Geological Survey Geophysical Investigations Map 988, 5 sheets, scale 1:500,000. [<https://doi.org/10.3133/gp988>]
- Gower, H. D.; Yount, J. C.; Crosson, R. S., 1985, Seismotectonic map of the Puget Sound region, Washington: U.S. Geological Survey Miscellaneous Investigations Series Map 1613, 1 sheet, scale 1:250,000, with 15 p. text. [<https://doi.org/10.3133/i1613>]
- Haugerud, R. A., 2009, Preliminary geomorphic map of the Kitsap Peninsula, Washington; version 1.0: U.S. Geological Survey Open-File Report 2009-1033, 2 sheets, scale 1:36,000. [<https://pubs.usgs.gov/of/2009/1033/>]
- Haugerud, R. A., 2021, Deglaciation of the Puget Lowland, Washington. In Waitt, R. B.; Thackray, G. D.; Gillespie, A. R., editors, *Untangling the Quaternary Period—A Legacy of Stephen C. Porter*: Geological Society of America Special Paper 548, p. 279–298. [[https://doi.org/10.1130/2020.2548\(14\)](https://doi.org/10.1130/2020.2548(14))]
- Heiskanen, W. A.; Vening-Meinesz, F. A., 1958, *The Earth and its gravity field*: McGraw-Hill Book Company, Inc., 470 p. [<https://www.science.org/doi/10.1126/science.129.3347.460.b>]

- International Association of Geodesy and Geophysics, 1971, Geodetic reference system 1967: International Association of Geodesy Special Publication No. 3, 116 p.
- Hunting, M. T., 1956, Inventory of Washington minerals; Part II—Metallic minerals: Washington Division of Mines and Geology Bulletin 37, Part II, 2 v. [https://www.dnr.wa.gov/Publications/ger_b37_part2_metallic_v1_1_foreword-germanium.pdf]
- Jeschke, D. A.; Eungard, D. W.; Troost, K. G.; Wisher, A. P., 2023, Subsurface database of Washington State—GIS data: Washington Geological Survey Digital Data Series 11, version 2.2, previously released February, 2019. [https://fortress.wa.gov/dnr/geologydata/publications/data_download/ger_portal_subsurface_database.zip]
- Logan, R. L.; Walsh, T. J.; Stanton, B. W.; Sarikhan, I. Y., 2009, Geologic map of the Maytown 7.5-minute quadrangle, Thurston County, Washington: Washington Division of Geology and Earth Resources Geologic Map GM-72, 1 sheet, scale 1:24,000. [http://www.dnr.wa.gov/Publications/ger_gm72_geol_map_maytown_24k.pdf]
- Mackin, J. H., 1944, Relation of geology to mineralization in the Morton cinnabar district, Lewis County, Washington: Washington Division of Mines and Mining Report of Investigations 6, 47 p., 2 plates. [https://www.dnr.wa.gov/Publications/ger_ri6_dmm_geol_mineralization_cinnabar_dist.pdf]
- McCaffrey, Robert; King, R. W.; Payne, S. J.; Lancaster, Matthew, 2013, Active tectonics of northwestern U. S. inferred from GPS-derived surface velocities: *Journal of Geophysical Research Solid Earth*, v. 118, p. 709–723. [<https://doi.org/10.1029/2012JB009473>]
- Morelli, Carlo, editor, 1974, The international gravity standardization net 1971: International Association of Geodesy Special Publication No. 4, 194 p.
- Mundorff, M. J.; Weigle, J. M.; Holmberg, G. D., 1955, Ground water in the Yelm area, Thurston and Pierce Counties, Washington: U.S. Geological Survey Circular 356, 58 p., 2 plates. [<https://doi.org/10.3133/cir356>]
- Nelson, A. R.; Personius, S. F.; Sherrod, B. L.; Buck, Jason; Bradley, Lee-Ann; Henley, Gary, II; Liberty, L. M.; Kelsey, H. M.; Witter, R. C.; Koehler, R. D.; Schermer, E. R.; Nemser, E. S.; Cladouhos, T. T., 2008, Field and laboratory data from an earthquake history study of scarps in the hanging wall of the Tacoma fault, Mason and Pierce Counties, Washington: U.S. Geological Survey Scientific Investigations Map 3060, 3 sheets, scale 1:30,000. [<http://pubs.usgs.gov/sim/3060/>].
- Nilsen, T. H., 1976, Washington Gravity Base Station Network: Washington Division of Geology and Earth Resources Circular 59, 83 p. [https://www.dnr.wa.gov/Publications/ger_ic59_wa_gravity_base_network.pdf]
- Noble, J. B.; Wallace, E. F., 1966, Geology and ground-water resources of Thurston County, Washington; Volume 2: Washington Division of Water Resources Water Supply Bulletin 10, v. 2, 141 p., 5 plates. [<https://apps.ecology.wa.gov/publications/SummaryPages/WSB10b.html>]
- Odum, J. K.; Stephenson, W. J.; Pratt, T. L.; Blakely, R. J., 2016, Shallow geophysical imaging of the Olympia anomaly: An enigmatic structure in the southern Puget Lowland, Washington State: *Geosphere*, v. 12, no. 5, p. 1617–1632. [<https://doi.org/10.1130/GES01248.1>]
- Phillips, J. D.; Hansen, R. O.; Blakely, R. J., 2007, The use of curvature in potential-field interpretation: *Exploration Geophysics*, v. 38, p. 111–119. [<https://doi.org/10.1071/EG07014>]
- Pierce County, WA, 2020, Pierce 2020 project, Pierce County, WA Lidar 2020, collected between April 10 and June 3, 2020 by Sanborn Map Company, Inc., 3-ft resolution, accessed April 16, 2023 [<http://lidarportal.dnr.wa.gov/>], metadata available on portal [<https://lidarportal.dnr.wa.gov/download?ids=1487>].
- Plouff, Donald, 2000, Field estimates of gravity terrain corrections and Y2K-compatible method to convert from gravity readings with multiple base stations to tide-and long-term drift-corrected observations: U.S. Geological Survey Open-File Report OF 00-140, 35 p. [<https://doi.org/10.3133/ofr00140>]
- Polenz, Michael; Alldritt, Katelin; Hehemann, N. J.; Sarikhan, I. Y.; Logan, R. L., 2009, Geologic map of the Belfair 7.5-minute quadrangle, Mason, Kitsap, and Pierce Counties, Washington: Washington Division of Geology and Earth Resources Open File Report 2009-7, 1 sheet, scale 1:24,000. [https://www.dnr.wa.gov/Publications/ger_ofr2009-7_geol_map_belfair_24k.pdf]
- Polenz, Michael; Hladky, F. R.; Bauer, A. L.; Lau, T. R.; Tepper, J. H.; Nesbitt, E. A.; Legorreta Paulin, Gabriel, 2023, Geologic map of the Bald Hill 7.5-minute quadrangle, Thurston, Pierce, and Lewis Counties, Washington: Washington Geological Survey Map Series 2023-03, 1 sheet, scale 1:24,000, with 37 p. text. [https://www.dnr.wa.gov/publications/ger_ms2023-03_geol_map_bald_hill_24k.zip]
- Polenz, Michael; Favia, J. G.; Hubert, I. J.; Legorreta Paulin, Gabriel; Cakir, Recep, 2015, Geologic map of the Port Ludlow and southern half of the Hansville 7.5-minute quadrangles, Kitsap and Jefferson Counties, Washington: Washington Division of Geology and Earth Resources Map Series 2015-02, 1 sheet, scale 1:24,000, with 40 p. text. [http://www.dnr.wa.gov/publications/ger_ms2015-02_geol_map_port_ludlow_hansville_24k.zip]
- Polenz, Michael; Hladky, F. R.; Anderson, M. L.; Alexander, K. A.; Tepper, J. H.; Miggins, D. P.; Legoretta Paulin, Gabriel, 2022, Geologic map of the McKenna and northern half of the Lake Lawrence 7.5-minute quadrangles, Thurston and Pierce Counties, Washington: Washington Geological Survey Map Series 2022-06, 1 sheet, scale 1:24,000, with 35 p. text. [https://www.dnr.wa.gov/publications/ger_ms2022-06_geol_map_mckenna_northern_lake_lawrence_24k.zip]
- Polenz, Michael; Hladky, F. R.; Anderson, M. L.; Tepper, J. H.; Horst, A. E.; Miggins, D. P.; Legoretta Paulin, Gabriel, 2021, Geologic map of the Tenalquot Prairie and northern two-thirds of the Vail 7.5-minute quadrangles, Thurston and Pierce Counties, Washington: Washington Geological Survey Map Series 2021-02, 1 sheet, scale 1:24,000, with 47 p. text. [https://www.dnr.wa.gov/publications/ger_ms2021-02_geol_map_tenalquot_prairie_northern_vail_24k.zip]
- Pratt, T. L.; Johnson, S. Y.; Potter, C. J.; Stephenson, W. J.; Finn, C. A., 1997, Seismic reflection images beneath Puget Sound, western Washington State: The Puget Lowland thrust sheet hypothesis: *Journal of Geophysical Research Solid Earth*, v. 102, no. B12, p. 27,469–27,489. [<https://doi.org/10.1029/97JB01830>]
- Pringle, P. T.; Goldstein, B. S., 2002, Deposits, erosional features, and flow characteristics of the late-glacial Tanwax Creek-Ohop Creek Valley flood—A likely source for sediments composing the Mima Mounds, Puget Lowland, Washington [abstract]: *Geological Society of America Abstracts with Programs*, v. 34, no. 5, p. A-89.
- Puget Sound Regional Council, 2005, Puget Lowlands 2005 project, collected in 2005 by Terrapoint, 3-ft resolution, accessed April 16, 2023 [<http://lidarportal.dnr.wa.gov/>], metadata available on portal [<https://lidarportal.dnr.wa.gov/download?ids=864>].
- San Juan, Charles, 2022, Natural background groundwater arsenic concentrations in Washington State: Study results: Washington Department of Ecology Publication No. 14-09-044, 72 p. [<https://apps.ecology.wa.gov/publications/SummaryPages/1409044.html>]
- Schasse, H. W., compiler, 1987, Geologic map of the Centralia quadrangle, Washington: Washington Division of Geology and Earth Resources Open File Report 87-11, 1 sheet, scale 1:100,000, with 28 p. text. [http://www.dnr.wa.gov/Publications/ger_ofr87-11_geol_map_centralia_100k.zip]
- Sisson, T. W.; Vallance, J. W.; Pringle, P. T., 2001, Progress made in understanding Mount Rainier's hazards: *Eos Transactions*, v. 82, no. 9, p. 113–120. [<https://doi.org/10.1029/01EO00057>]

- Snively, P. D., Jr.; Roberts, A. E.; Hoover, Linn, Jr.; Pease, M. H., Jr., 1951, *Geology of the eastern part of the Centralia-Chehalis coal district, Lewis and Thurston Counties, Washington*: U.S. Geological Survey Coal Investigations Map 8, 2 sheets, scale 1:31,680. [<https://doi.org/10.3133/coal8>]
- Snively, P. D., Jr.; Brown, R. D., Jr.; Roberts, A. E.; Rau, W. W.; Schopf, J. M., 1958, *Geology and coal resources of the Centralia-Chehalis district, Washington*: U.S. Geological Survey Bulletin 1053, 159 p., 6 plates. [<https://doi.org/10.3133/b1053>]
- Swick, C. H., 1942, *Pendulum gravity measurements and isostatic reductions*: U.S. Coast and Geodetic Survey Special Publication No. 232, 82 p.
- Tacoma–Pierce County Health Department, 2023, *Pierce County water quality* [webpage]: Tacoma–Pierce County Health Department. [accessed March 15, 2023, at <https://piercecowa.maps.arcgis.com/apps/webappviewer/index.html?id=ea09ff7335974c20b89590db2586bf84>]
- Telford, W. M.; Geldart, L. P.; Sheriff, R. E., 1990, *Applied Geophysics*. Cambridge University Press, 770 p.
- Troost, K. G., 2016, *Chronology, lithology and paleoenvironmental interpretations of the penultimate ice-sheet advance into the Puget Lowland*, Washington State: University of Washington Doctor of Philosophy thesis, 239 p.
- U.S. Geological Survey, 2016, *SWWA foothills 2017 project, Western Washington 3DEP lidar*, collected between Mar. 17 and Sept. 30, 2016 by Quantum Spatial Inc., 3-ft resolution, accessed April 16, 2023 [<http://lidarportal.dnr.wa.gov/>], metadata available on portal [<https://lidarportal.dnr.wa.gov/download?ids=1079>].
- Utah State University Luminescence Lab, 2022, *How to sample* [webpage]: Utah State University. [accessed Oct. 3, 2022, at <https://www.usu.edu/geo/osl/how-to-sample>]
- Van Wagoner, T. M.; Crosson, R. S.; Creager, K. C.; Medema, G. F.; Preston, L. A.; Symons, N. P.; Brocher, T. M., 2002, *Crustal structure and relocated earthquakes in the Puget Lowland, Washington, from high-resolution seismic tomography*: *Journal of Geophysical Research Solid Earth*, v. 107, no. B12, p. ESE 22-1–ESE 22-23. [<https://doi.org/10.1029/2001JB000710>]
- Walsh, T. J.; Logan, R. L.; Polenz, Michael; Schasse, H. W., 2003, *Geologic map of the Nisqually 7.5-minute quadrangle, Thurston and Pierce Counties, Washington*: Washington Division of Geology and Earth Resources Open File Report 2003-10, 1 sheet, scale 1:24,000. [https://www.dnr.wa.gov/publications/ger_ofr2003-10_geol_map_nisqually_24k.pdf]
- Wallace, E. F.; Molenaar, Dee, 1961, *Geology and ground-water resources of Thurston County, Washington, volume 1: Washington Division of Water Resources Water Supply Bulletin 10*, v. 1, 254 p., 2 plates.
- Walters, K. L., 1965, *Mashel Formation of southwestern Pierce County, Washington*. In Cohee, G. V.; West, W. S., *Changes in stratigraphic nomenclature by the U.S. Geological Survey, 1964*: U.S. Geological Survey Bulletin 1224-A, p. 55–59. [<https://doi.org/10.3133/b1224A>]
- Walters, K. L.; Kimmel, G. E., 1968, *Ground-water occurrence and stratigraphy of unconsolidated deposits, central Pierce County, Washington*: Washington Department of Water Resources Water Supply Bulletin 22, 428 p., 3 plates. [<https://fortress.wa.gov/ecy/publications/SummaryPages/WSB22.html>]
- Wells, R. E.; McCaffrey, Robert, 2013, *Steady rotation of the Cascade arc*: *Geology*, v. 41, no. 9, p. 1027–1030. [<https://doi.org/10.1130/G34514.1>]
- Wells, Ray; Bukry, David; Friedman, Richard; Pyle, Doug; Duncan, Robert; Haeussler, Peter; Wooden, Joe, 2014, *Geologic history of Siletzia, a large igneous province in the Oregon and Washington Coast Range: Correlation to the geomagnetic polarity time scale and implications for a long-lived Yellowstone hotspot*: *Geosphere*, v. 10, no. 4, p. 692–719. [<https://doi.org/10.1130/GES01018.1>]
- Washington Geological Survey, 2019, *Oil and gas wells—GIS data*: Washington Geological Survey Digital Data Series 21, version 3.4, previously released July, 2016. [https://fortress.wa.gov/dnr/geologydata/publications/data_download/ger_portal_oil_gas_wells.zip]
- Washington Geological Survey, 2023, *Geophysics Database—GIS data*: Washington Geological Survey Digital Data Series 28, version 1.0, April 2023. [https://fortress.wa.gov/dnr/geologydata/publications/data_download/ger_portal_geophysics.zip]
- Washington State Department of Ecology, 2022, *Washington State well log viewer—Text search or map search* [webpage]: Washington State Department of Ecology. [accessed May 17, 2022, at <https://fortress.wa.gov/ecy/wellconstruction/map/wclwebMap/default.aspx>]
- Washington Department of Natural Resources, 2021, *Thurston 2021 project, Thurston County, Washington Lidar Technical Data Report*, collected between March 27 and April 3, 2021 by NV5 Geospatial Corvallis, 3-ft resolution, accessed April 16, 2023 [<http://lidarportal.dnr.wa.gov/>], metadata available on portal [<https://lidarportal.dnr.wa.gov/download?ids=1517>].
- Washington State Department of Health, 2014, *Arsenic and your private well*: Washington State Department of Health pamphlet 334-156, 2 p. [<https://doh.wa.gov/sites/default/files/legacy/Documents/Pubs/334-156.pdf?uid=643d80c503f26>]

Appendix A. Geophysical Methods

GRAVITY

Overview and Purpose

Lateral changes in isostatic gravity across a region result from density changes within rocks of the mid-to-upper crust. Gridding gravity measurements creates a map that outlines areas of high gravity and low gravity. Areas of high gravity indicate that high-density rocks (for example, many igneous and metamorphic rocks) are closer to the surface. Areas of low gravity indicate less-dense material near the surface, such as sediment within a basin. Gravity surveys are especially useful in delineating steeply dipping contacts between two rock bodies that have a large contrast in density. Gravity data constrained with measured rock densities allow us to create models of the subsurface geology that quantitatively predict observed data.

Description of Method

FIELD METHODS AND SAMPLED LOCATIONS

Measurements represent a combination of 347 new gravity stations collected using a Scintrex CG-6 meter (Serial # 19050174), the PACES database (now defunct; data obtained from B. Drenth, U. S. Geological Survey, written communication, 2020); Polenz and others (2021, 2022); and a WGS unpublished dataset. We utilize base station ‘OLYK’ with ties to Chehalis B (Nilsen, 1976) and Johnston Ridge Observatory (Washington Geological Survey, 2023) to tie our data to the U.S. gravity network.

Gravity station spacing at roughly 2 km generates a basic grid over a large area. In areas where known structures exist or initial gravity data collection showed a significant gradient, station spacing is 1 km to provide greater resolution. Forty-nine new bedrock density samples and 316 magnetic susceptibility measurements collected from exposed bedrock provide ground-truth for map interpretation and constrain geophysical modeling.

DATA REDUCTION AND PROCESSING

A Javad Triumph-2 differential GPS unit provided the horizontal and vertical position of each station. Horizontal positions are then used to pull elevations from areas with high-quality lidar. We apply the factory instrument (gravimeter) calibration constants to each gravity observation, apply correction factors obtained from the Mount Hamilton calibration loop east of San Jose, CA (Barnes and others, 1969), and correct for Earth tides to produce observed gravity values. The data reference is the International Gravity Standardization Net of 1971 (Morelli, 1974), and the reference ellipsoid is the Geodetic Reference System of 1967 (International Association of Geodesy and Geophysics, 1971).

Gravity data reduction formulas for the free-air anomaly are standard (for example, Telford and others, 1990; Swick, 1942) and we applied Bouguer, Earth curvature, and terrain corrections out to 166.7 km from each station to produce a complete Bouguer anomaly. Terrain corrections are a combination of a field-based component (to a radius of 68 m using the Hayford system; Plouff, 2000). The complete Bouguer anomaly is further reduced to an isostatic anomaly using an Airy-Heiskanen model (Heiskanen and Vening-Meinesz, 1958) that produces the isostatic correction, assuming a 25-km-thick crust at sea level and a crust-mantle density contrast of 400 kg/m³. All parts of the data reduction process assume a standard reduction density of 2,670 kg/m³. Average uncertainty in steep and hilly regions is 0.12–0.23 mGal, whereas average uncertainty in flatter areas is 0.05–0.1 mGal.

The minimum-curvature algorithms in the GIS software package Geosoft Oasis Montaj transform our point isostatic anomaly data into gridded surfaces. The maximum horizontal gradients (referred to as ‘max-spots’) calculated using the curvature analysis methodology of Phillips and others (2007) quantitatively locate strong and linear boundaries between rocks in the subsurface that have substantial density differences.

HAND SAMPLE DENSITIES

We collected bedrock samples throughout the study area for laboratory analysis. We weighed samples using an A & D company limited FX-3000i WP analytical balance. Three measurements per sample combine to determine density: a dry weight in air, a submerged (water-saturated) weight, and a water-saturated weight in air. While these measurements produce grain density, saturated bulk density, and dry bulk density, saturated bulk density best reflects subsurface conditions and was therefore referenced for modeling.

GEOMAGNETICS

Overview and Purpose

Magnetic surveys map the changes in the earth’s magnetic field due to local magnetic sources at high resolution. This method delineates contacts between geologic units of contrasting magnetic properties, particularly in the mid to upper crust. A large number

of magnetic profiles help to precisely determine magnetic contacts and trace them across a map area. Individual profiles, coupled with magnetic susceptibility measurements of surficial rocks, are powerful geophysical constraints for 2D subsurface modeling.

Description of Method

Aeromagnetic data used in this study were acquired in 1995 and 2016 (Blakely and others, 1999, 2020) via low-flying aircraft with a stinger-mounted magnetometer. For the 1995 survey, north–south flight lines are 0.4 km apart, with east–west tie lines spaced at 8 km. For the 2016 survey, east–west flight lines are 0.4 km apart and north–south tie lines at 4 km spacing. Aeromagnetic measurements were interpolated to a projected, rectilinear grid using a bi-directional gridding algorithm within the GIS software package Geosoft Oasis Montaj. Another filter reduces this anomaly to the magnetic pole, more closely centering anomalies over their sources for map-view interpretation. We apply a filter to the aeromagnetic map to enhance short-wavelength anomalies from shallower sources (termed ‘residual’). The residual results from subtracting a version of the original aeromagnetic grid that has been filtered (upward continued 50 m to enhance long-wavelength anomalies) from the original grid. The residual retains short-wavelength anomalies that mainly reflect the effects from sources in the upper couple kilometers of the crust. This method does not produce anomalies reflecting a precise depth of sources, but can separate out anomalies sourced generally deeper or shallower. The same algorithm used to determine the gravity max-spots is applied to residual grids to quantitatively locate strong and linear gradients (lineaments) that correspond to sharp and linear subsurface geologic boundaries.

HAND SAMPLE SUSCEPTIBILITIES

Magnetic susceptibility measurements taken with a KT10 Kappa Meter accompany rock sample density measurements, and we use the same meter to collect direct readings from outcrops where possible. Weathering tends to replace denser minerals with less dense weathering products and turn magnetite into less magnetic minerals like hematite. Therefore, all of our measured rock densities and susceptibilities from surface outcrops (see Data Supplement) can be considered minimum values.

CALCULATED VOLUME SUSCEPTIBILITIES FROM CUTTINGS

Overview and Purpose

Volume susceptibility measures the magnetic susceptibility of a specific volume of rock regardless of sample size. Attempts to measure volume susceptibility on small cutting samples yield susceptibility measurements much lower than would be measured on an outcrop, a result of the instrument sampling a smaller volume of material than available in an outcrop. In this study, we convert volume susceptibility measurements of small samples to mass susceptibility following Ali and others (2015), as described below, then use a standard to convert the mass back to a corrected volume susceptibility. The advantage of measuring mass magnetic susceptibility is that it removes any effects due to anomalous porosity, which can affect the volume magnetic susceptibility measurements. This includes the intrinsic porosity of the individual drill cuttings and the porosity of the vial of very small samples caused by vacant space between cuttings. Drill cuttings of different sizes with an identical mineralogy will give exactly the same mass magnetic susceptibility value after this conversion.

Description of Method

Twelve empty 5 ml plastic vials were weighed using an analytical balance (Sartorius model CPA324S). We determined sample weight and bulk density by measuring vials filled with cuttings at selected representative depths from the Willhoite well. Volume susceptibility measurements made using the KT10 Kappa Meter applied to the filled plastic vials divided by the bulk density yielded a mass susceptibility. We selected three hand sample standards collected at the surface (volcaniclastic, andesitic, and basaltic) by matching lithologies interpreted to be representative from the well log. We processed samples using a chipmunk crusher and sieving to yield sample grains similar in size to cuttings from the well. The mass susceptibility of these standards was then measured in the same manner as the oil well cuttings. A coefficient was calculated from the standards that allowed a conversion from an oil cutting mass susceptibility to a calculated volume susceptibility. The calculated volume susceptibility of cutting samples then constrained our modeling interpretations of material at depth.

QUANTITATIVE CROSS-SECTION MODELING

Overview and purpose

Quantitative 2-D forward modeling of cross sections constrained by potential-field data provides insight into subsurface unit and structure geometry that goes beyond qualitative interpretations of map-view data. This technique helps provide the best possible interpretations of structure types (for example normal, reverse, or strike-slip faults), fault or contact dips in the upper crust (for example steep or shallow), and offset across faults on units with particularly strong physical-property contrasts with surrounding rocks. This method also can identify blind faults that have little surface expression and are difficult to capture via surface geology observations.

Description of Method

GM-SYS provides the platform for computing the sum effect of blocks of rock in the subsurface in a 2-D cross section on both the gravitational and geomagnetic fields of the Earth. This is a forward-modeling method. This means the operator hypothesizes which rock types are in the subsurface, their location, and their volume, and the GM-SYS program predicts the total fields that result from that particular model. The operator's responsibility is to refine the hypothesis until the predicted potential-fields match the data measured in the field. This ensures that any cross-section interpretation of the subsurface matches two additional data types (for example gravity and magnetism) besides the geology, and thus reduces the number of potential hypotheses for the subsurface geometry of rocks.

Several types of data constrain this process in addition to the gravity and aeromagnetic data. Surface geologic observations define rocks that are in the model's near-surface topography, and lab measurements (see above) of density and magnetic properties of hand samples gathered from the surface provide additional rock property constraints. Also essential is the knowledge of the operator and collaborators in the project about the geologic history, expected stratigraphy in the subsurface, and structural geometries that are physically possible based on standard geologic mapping and cross-section construction techniques.

Within these constraints, there is still the strong possibility that multiple hypotheses of subsurface geometry can fit the gravity and magnetic data within the accepted error for those two data types. Therefore, care in the construction of models helps define which parts of the subsurface model are well-constrained with the fewest alternative hypotheses and which parts could have multiple possible geometries. In general, potential-field data provide strong constraint (including their position and dip) on simple, steeply dipping boundaries that juxtapose rocks with strong differences in physical properties. Potential-field data provide very poor constraint on horizontal boundaries or boundaries between rocks with little contrast in physical properties. Depth of sub-horizontal contacts within sedimentary rocks is particularly suspect and is never well-constrained without the addition of good quality well or reflection-seismic data. The depth of sub-horizontal contacts between units with strongly contrasting properties is resolvable but depends on uncertainties in the physical properties of those units. In those cases, the modeled depth of a contact can be highly sensitive to changes in the assumed density or magnetism of the rocks on either side of the contact.

Our approach first constructs initial simplified models, including uniform packages of sediment, sedimentary rock, metamorphic rock, or volcanic rock to fit the overall long-wavelength features in the gravity and magnetic data. Our model space extends beyond the end of the models shown in this report to avoid edge effects due to truncated subsurface volumes. Adding detail in the stratigraphy and decreasing the size of blocks after the major fit allows modeling of smaller-scale features that fit shorter wavelength anomalies, particularly near the surface. During each iteration, we test possible options for physical properties of rocks and geometries of boundaries permitted by the surface geology observations and measured rock-property constraints. Throughout the process of testing many variables, we concluded that there was a good fit if each model iteration produced a similar solution to fit the data.

Appendix B. Luminescence Age Estimates

OVERVIEW AND PURPOSE

Luminescence dating estimates the time that has passed since sandy (or silty) sediment was deposited. Following sediment deposition, environmental irradiation causes electrons in feldspar grains to jump into a metastable, higher-energy spin cycle. The technique assumes that this occurs at a constant rate, such that older sediment contains proportionately more electrons in elevated spin cycles. The technique functions by measuring how much light electrons emit when released from their elevated spin cycle. This is done by subjecting the sample to infrared light that knocks the electrons out of their metastable spin cycle; their return to a lower-energy spin cycle emits light. The amount of light emitted is proportional to the time since deposition of the sample—meaning that more light is indicative of an older sample.

SAMPLE COLLECTION AND PREPARATION

We followed online instructions from Utah State University's Luminescence Lab on how to sample (Utah State University Luminescence Lab, 2022). Samples for luminescence dating need to be collected from sediment that has not been exposed to light since its time of deposition, so the samples need to be recovered without being exposed to light. To do this, we first removed at least 15 cm of sand from an exposure and then pounded a 4.5-cm diameter, 25-cm-long steel tube into the in-place sediment. The tube was retrieved by digging out the surrounding material. This removed material was collected in plastic bags for moisture and bulk dose rate measurements used for calibration. The sample tube was packed with Styrofoam spacers (if needed) and sealed with duct tape and labeled. The lab analyzed sand in the core of the tube, which had not been exposed to light since deposition.

LUMINESCENCE ANALYSIS METHODS

Our samples were analyzed by the USGS Luminescence Dating Laboratory in cooperation with the U.S. Bureau of Reclamation, and a detailed report on their methods is in the Data Supplement.

RESULTS

We collected and analyzed three sand samples from the map area. Summary data are in Tables 1 and B1; full analytical data are in the Data Supplement.

Table B1. Optically Stimulated Luminescence (OSL) and Infrared Stimulated Luminescence (IRSL) results from age sites GD1, GD5, and GD6. Processed and analyzed by Shannon Mahan, USGS Luminescence Dating Laboratory.

Site ID	GD1	Fine- to medium-grained sand with silt and rare pebbles sampled 1 m below ground surface at the base of a gradual, north-facing slope in the northern portion of the map area. Sand is loose and medium brown in color. Sand grains are angular to subangular. Deposit appears structureless. The north-facing slope was likely eroded by the Cordilleran ice-sheet ~15 ka and the outcrop we sampled is exposed in an old road cut (<50 years old). Sand contains quartz, multicolored lithics, and minor mafic grains. Sampled Oct. 3, 2022, by Trevor Contreras and Rebecca Goughnour.
Field sample ID	HLB-30-1	
Map unit	Qps	
TRS location	Sec. 3, T17N R3E	
Latitude (degrees)	46.99458	
Longitude (degrees)	-122.40469	
Elevation (ft)	492	
Age (ka) $\pm 2\sigma$		80.18 ± 7.5

Site ID	GD5	Medium- to coarse-grained sand layer sampled 2.5 m below ground surface. Sand layer is ~1 m thick and overlain by a cobbly diamicton that we interpret to be a lahar deposit. The outcrop is exposed in a building pad that was cut into a southeast-facing slope ~25 years ago. Approximately 15 ka, the Puget Lobe of the Cordilleran ice-sheet deposited ~3 m of glacial drift on top of the sampled lahar deposits. Sand contains abundant subhedral to anhedral plagioclase crystals, igneous lithic grains, and mafic crystals. Some bioturbation was noted (0.5 cm horizontal burrow holes) at the sampled outcrop, but we attempted to avoid these areas for our sample. Sampled Oct. 4, 2022, by Trevor Contreras and Rebecca Goughnour.
Field sample ID	HLB-31-3	
Map unit	Qpc	
TRS location	Sec. 12, T16N R3E	
Latitude (degrees)	46.88943	
Longitude (degrees)	-122.38003	
Elevation (ft)	735	
Age (ka) $\pm 2\sigma$		30.38 ± 5.18

Table B1. Continued.

Site ID	GD6	<p>Coarse to medium-grained sand layer sampled 12 m below ground surface. Sand lens is ~28 cm thick and overlain by a bouldery diamicton that we interpret to be a lahar deposit from Mount Rainier. The outcrop was cut into a southwest-facing slope more than 50 years ago along an old road that descends to the Nisqually River. Note: this location is just west of the quadrangle boundary and is not shown on the map plate.</p> <p>Sampled Sept. 7, 2022, by Trevor Contreras and Rebecca Goughnour</p>
Field sample ID	HLB-22-3	
Map unit	Qpc	
TRS location	Sec. 36, T17N R2E	
Latitude (degrees)	46.91120	
Longitude (degrees)	-122.50060	
Elevation (ft)	129	
Age (ka) $\pm 2\sigma$		24.12 \pm 4.65